SCREENING AND DISCOVERY OF METAL COMPOUND ACTIVE SITES FOR STRONG AND SELECTIVE ADSORPTION OF N_2 IN AIR

A PREPRINT

Nianhan Tian[1], Benjamin M. Comer[2], Andrew J. Medford[1] †
Department of Chemical and Biomolecular Engineering
Georgia Institute of Technology
[2] SUNCAT Center for Interface Science and Catalysis
SLAC National Accelerator Laboratory
† *Corresponding author: Andrew J. Medford, ajm@gatech.edu*

October 27, 2023

ABSTRACT

Photocatalytic nitrogen fixation has the potential to provide a greener route for producing nitrogen-based fertilizers under ambient conditions. Computational screening is a promising route to discover new materials for the nitrogen fixation process, but requires identifying "descriptors" that can be efficiently computed. In this work, we argue that selectivity toward the adsorption of molecular nitrogen and oxygen can act as a key descriptor. A catalyst that can selectively adsorb nitrogen and resist poisoning of oxygen and other molecules present in air has the potential to facilitate the nitrogen fixation process under ambient conditions. We provide a framework for active site screening based on multifidelity density functional theory (DFT) calculations for a range of metal oxides, (oxy)borides, and (oxy)phosphides. The screening methodology consists of initial low-fidelity fixed geometry calculations and a second screening in which more expensive geometry optimizations were performed. The approach identifies promising active sites on several TiO_2 polymorph surfaces and a VBO_4 surface, and the full nitrogen reduction pathway is studied with the BEEF-vdW and HSE06 functionals on two active sites. The findings suggest that other TiO_2 polymorphs may play a role in photocatalytic nitrogen fixation, and that VBO_4 may be an interesting material for further studies.

Keywords ammonia synthesis · in silico screening · titanium dioxide

1 Introduction

The production of ammonia (NH_3) from atmospheric nitrogen on an industrial scale is accomplished through the Haber-Bosch process [1], which has been called the most important invention of the 20$^{\text{th}}$ century [2]. As the main ingredient in nitrogen-based fertilizers, ammonia has directly helped increase food production, enabling the global population to nearly quadruple in the early 20$^{\text{th}}$ century [2]. Despite its impressive positive impact on fertilizer production, the Haber-Bosch process is energy and emissions intensive [3–5]. Emitting 340 million tonnes of CO_2 equivalent per year and consuming 2.5 exajoule energy per year, ammonia synthesis has become one of the most carbon and energy intensive processes in the chemical industry [5–8]. The cost of energy consumption is mainly controlled by the production of molecular hydrogen and nitrogen feedstocks [5,9,10]. Molecular hydrogen is produced via methane steam reforming that contributes to 340 million tonnes of CO_2 equivalent per year [11]. Molecular nitrogen is obtained from cryogenic distillation, which requires 6.9 kJ per mol N_2 [12]. Furthermore, the highly centralized ammonia production process leads to high distribution costs and inequitable distribution of fertilizers throughout the world, especially in developing areas [13–15]. These downsides of the Haber-Bosch process push the need to develop alternative catalytic systems that enable sustainable and economical fixed nitrogen production in a distributed manner.

Photo(electro)catalytic nitrogen fixation has the potential to produce ammonia under ambient conditions [16–24]. Photocatalytic ammonia synthesis has shown particular promise as a low capital and highly distributed alternative [5], but

current efficiencies indicate that significant additional research is required. Current progress on photocatalytic nitrogen fixation has provided valuable insights regarding the mechanism at a molecular scale. One of the first computational studies of photocatalytic nitrogen fixation was performed by Comer and Medford[7]. This theoretical study explored both dissociative and associative nitrogen reduction on rutile (110) TiO_2 active sites, including pristine, oxygen vacancies and iron substitution sites using density functional theory (DFT). However, the results indicated a thermodynamic barrier that is higher than the conduction band edge of rutile TiO_2. The interaction between surface hydroxyl groups and nitrogen radicals was also explored in a theoretical study by Xie et al[25]. It was suggested that the hydroxyl groups produced by surface hydroxylation of water[26–30] on titania surfaces could drive the nitrogen reduction process, although no direct experimental evidence was provided. An alternative hypothesis proposed by Comer et al. in a study based on ambient pressure X-ray photoelectron spectroscopy and DFT calculations[31], where a carbon substitution site on rutile TiO_2 and demonstrated a thermodynamically feasible carbon-assisted nitrogen reduction reaction (NRR) pathway. Building on this observation, Huang et al.[32] used electron paramagnetic resonance, infrared spectroscopy, and DFT to show that radical species derived from methanol also interact with nitrogen, providing a more detailed perspective on carbon-assisted nitrogen dissociation.

Despite current progress in probing the mechanistic pathway of photo(electro)catalytic NRR, these mechanisms typically assume a pure nitrogen feedstock, and issues of competitive adsorption in the presence of molecular oxygen have not been explored. To achieve the ultimate goal of NRR under ambient conditions, it will be critical to reduce the need for air separation[5]. As mentioned above, the cost of high-purity nitrogen from cryogenic distillation in the Haber-Bosch process accounts for approximately 25% of the total capital cost of the entire plant[33]. In the Haber-Bosch process, high purity nitrogen is required to preserve the catalyst and prevent ammonia oxidation[34]. Furthermore, industrial catalysts used in the process can be poisoned by oxygen or hydroxyl groups below industrial conditions (700 K, 100 bar)[35,36]. Catalyst poisoning severely hinders the rate of production, which is even more pronounced when water vapor is present[35]. Similar phenomena were observed in photocatalytic and electrocatalytic nitrogen fixation experiments. The photocatalytic activity of rutile TiO_2 in air has been reported to be reduced by 65% compared to a high-purity nitrogen environment[37]. Under ambient conditions, oxygen can react with photogenerated electrons and holes and turn into reactive oxygen species, decreasing the conversion efficiency[31,38,39]. Remarkably, a recent study from the electrocatalysis community showed that the Faradaic efficiency and stability of a lithium-mediated NRR can actually be improved by adding small amounts of oxygen, which limits excessive lithium reduction by decreasing the lithium diffusion rate[40]. This is a promising result, but the small amounts of oxygen that enhance the NRR will likely be hard to control and will require further experiments and scale-up studies to assess feasibility. If a nitrogen fixation process is not resistant to contamination from oxygen and other common components under ambient conditions, investment in air separation will be unavoidable and will likely become the dominant capital cost[5]. Hence, discovering photocatalysts that are directly compatible with air or low-purity nitrogen is an important step towards enabling the photocatalytic NRR process under ambient conditions[5,6]. Furthermore, finding materials that can selectively adsorb N_2 over O_2 presents a fundamental chemistry challenge, given the relatively high reactivity of O_2 compared to N_2. These materials may prove interesting as case studies in fundamental chemistry or find applications in other fields such as air separations.

In this work, we propose that the selectivity of adsorbing nitrogen over oxygen is an interesting descriptor of the performance for photocatalytic ammonia synthesis under ambient conditions. Adsorption of N_2 is a necessary condition for any N_2 conversion process, regardless of the mechanism, so selective adsorption of N_2 is a necessary (but not sufficient) condition for aerobic photocatalytic synthesis of ammonia. Employing DFT enables surface adsorption energy calculations, which can be used to predict adsorption selectivity. We quantify the selectivity by comparing the nitrogen and oxygen adsorption free energy on the active site. The inert nature of nitrogen means that many surfaces will not bind it strongly, and if a surface can stably adsorb a nitrogen molecule, it is likely that it can adsorb oxygen even more strongly. Furthermore, this descriptor also provides an implicit approximation of the (meta)stability of a given active site, since extremely unstable active sites are likely to react more strongly with oxygen than nitrogen, particularly for oxides. Therefore, the descriptor will identify metastable active sites with an abnormally strong reactivity toward N_2, which we hypothesize will correlate with low barriers for conversion of N_2 to ammonia.

Naturally, a thorough description of the photocatalytic performance of a material would require detailed analyses of surface stability, high coverage thermodynamics and reaction barriers, and microkinetic modeling[41,42]. However, these analyses require a significant amount of resources, which makes them impractical to scale to large search spaces of materials[43]. Thus, it is often most efficient to utilize relatively simple binding energy descriptors to narrow down the catalyst search space and follow up with more detailed studies of the most promising materials and surfaces.

In this study, we started with 516 bulk structures of metal oxides, borides, and phosphides from the Materials Project[44] as candidate photocatalysts. Then, low Miller index (i.e. 100, 101, 001 and 111) surfaces were generated from each bulk structure. Adsorbate-slab configurations were generated for every active site on a surface. To screen these candidate active sites, we used a two-stage screening strategy. In the first round of low-fidelity screening, we calculate nitrogen and oxygen adsorption energies while holding slab atoms in fixed positions. We then used the binding energy

descriptors from low-fidelity calculations to guide the selection of calculations that allowed for surface relaxation and reconstruction. We refer to these subsequent calculations as the "second round screening" throughout this paper. Allowing surface relaxations on metal compounds led to substantial surface reconstructions and significantly weaker N_2 adsorption energies in most cases, suggesting that the approach of using a fixed slab is more likely to produce false positives than false negatives, and indicating the importance of considering relaxations in future screening studies. Strong and selective N_2 adsorption was observed in three active sites even after the second round of screening.

Remarkably,two of the three identified sites occur on uncommon polymorphs (space group $P3_121$ and C2/m) of TiO_2, which is one of the most commonly reported catalysts for photocatalytic ammonia synthesis. The other site is on VBO_4 (space group $P2_{1/c}$), a material that has not yet been tested for photocatalytic ammonia synthesis. In our detailed investigation, we focused on the (001) surface of a meta-stable trigonal TiO_2 $P3_121$ polymorph[45], which demonstrated the highest selectivity for N_2 among the TiO_2 sites, and the (100) surface of VBO_4. Using both BEEF-vdW and HSE06 functionals, we performed an extensive thermodynamic analysis of the NRR pathway on these two active sites. The results confirmed that these surfaces show strong and selective reactivity toward N_2 and have thermodynamic barriers similar to the (110) rutile TiO_2 surface, indicating that other polymorphs of TiO_2 may play a role in photocatalytic ammonia synthesis, and that VBO_4 may be a promising material for further experimental investigations.

2 Methods

2.1 DFT calculations

In this work, we used both generalized gradient approximation (GGA) and hybrid level calculations to simulate the electronic structure of relevant slab systems. It has been widely suggested that the catalytic properties of TiO_2 can be appropriately treated with GGA functionals,[46–48], while hybrid methods have shown promising results when describing the detailed electronic and band structure of various polymorphs and nanoparticles of TiO_2[49,50]. Thus, we utilize the BEEF-vdW[51] GGA functional for all high-throughput screening and geometry optimizations, and we utilize single-point HSE06 calculations to evaluate the energetics of the most promising active site.

All GGA functional calculations and geometry optimizations were performed in the Quantum ESPRESSO software package[52,53] together with the Atomic Simulation Package (ASE)[54]. Uncertainty estimation due to the GGA approximation for each calculation was obtained from the ensemble of values produced by BEEF-vdW. The plane-wave cutoff energy was set at 600 eV for all GGA calculations, and a Monkhorst-Pack k-point grid spacing of $4 \times 4 \times 1$ was used for all slab models[55]. The Standard Solid State Pseudopotentials (SSSP) efficiency set[56] was chosen to treat core-electron interactions. Spin polarization and dipole corrections[57] were applied to all GGA slab calculations. All geometries were optimized using the BFGS line search method with a maximum total force of 0.05 eV/Å. Gas phase calculations were performed at the Γ point in a unit cell with 6 Å vacuum with all other settings identical to slab calculations. Geometries of adsorbed surfaces were determined by trying adsorbates at multiple orientations and taking the lowest-energy configuration.

We used the Heyd-Scuseria-Ernzerhof functional (HSE06)[58] to more accurately probe the energetics of the complete associative ammonia synthesis mechanism on the most promising trigonal TiO_2 (001) and VBO_4 (100) active sites. HSE06 calculations were performed in the Simulation Package for Ab-initio Real-space Calculations (SPARC) software package[59–67]. Soft and transferable pseudopotentials from multi-objective optimization (SPMS)[62] were used as the potential corresponding to the nucleus and core electrons. The Monkhorst-Pack k-point grid of $4 \times 4 \times 1$ and a mesh spacing of 0.1 Å, corresponding to an approximate plane-wave cutoff of 1800 eV[68,69], were used. For slab calculations, periodic and Dirichlet boundary conditions were prescribed in the plane and perpendicular to the plane of the slab, respectively. For gas phase molecules calculations, Dirichlet boundary conditions are employed in all three coordinate directions. The convergence tolerance on the normalized residual of electron density of the SCF iteration was set at 10^{-6}. The convergence tolerance on the Fock energy was set at 10^{-4} Hartree. The maximum number of Fock iterations was 20. The hybrid range screening parameter was set at 0.106 $Å^{-1}$ [58,70]. The parameters of all DFT simulations with both codes and exchange-correlation functionals are selected such that the numerical error is expected to be below 0.025 eV.

We also computed the free energies of adsorption for the relevant adsorbed intermediate states on the specific trigonal TiO_2 (001) and VBO_4 (100) surfaces. Since DFT calculates energies at 0 K in a perfect vacuum, we must add zero-point energy (ZPE) and thermal corrections. To include ZPE and thermal contributions, vibrational frequency calculations and statistical mechanics corrections were performed using the BEEF-vdW level fo theory and the ASE thermochemistry implementations. The ground state electronic energies (E_{ele}) calculated by DFT were converted to free energies (G_i^o) using the following equation:

$$G_i^o = E_{ele} + E_{ZPE} + \Delta H - T\Delta S \tag{1}$$

where E_{ZPE} is the zero point energy, ΔH and $T\Delta S$ are thermal contributions. Gas phase molecules were treated as ideal gases and adsorbates were treated with the harmonic approximation with a low-frequency cutoff of 30 cm^{-1} [71]. Relative free energies were computed with respect to reference states using the formula [72]:

$$G_i = G_i^o - \sum_j n_j \mu_j \tag{2}$$

where G_i is the free energy of species i, G_i^o is the total energy computed from DFT and free energy corrections, n_i is the number of atoms j in species i, and μ_j is the reference chemical potential. The reference for nitrogen was N_2 ($\mu_N = \frac{1}{2}G^o_{N_2}$), the reference for hydrogen was H_2 ($\mu_N = \frac{1}{2}G^o_{H_2}$), and the reference for oxygen was O_2 ($\mu_O = \frac{1}{2}G^o_{O_2}$). All thermodynamics were evaluated at 300 K. Gas partial pressures were set to approximate atmospheric conditions (0.8 atm N_2, 0.2 atm O_2). No gas-phase electronic corrections are applied.

2.2 Material Screening

We used the Materials Project [44] online database to obtain a pool of bulk metal oxide structures. For this study, we chose transition metal oxide, (oxy)boride, and (oxy)phosphide species containing Sc, Ru, V, Sn, Nb, Zr, Mo, and Ti (nonmagnetic metals that are commonly active for nitrogen chemistry in heterogeneous and homogeneous catalysis [73–84]). We included borides and phosphides due to the fact that boron is known to interact strongly with nitrogen [85,86], and phosphorus is a nutrient that is commonly used in fertilizers and thus phosphides may have practical advantages for fertilizer production. The targeted band gap of the material was set at 0.1 eV to 5.0 eV to identify materials that may be effective photocatalysts. The range was intentionally chosen to be very wide due to well-known errors of GGA functionals in estimating band gaps. There were 516 bulk structures from Materials Project with unique space groups that met these conditions at the time queried, and a full list of bulk structures is given in the SI. From the pool of bulk structures, we generated surfaces from the low Miller index facets (i.e. 100, 101, 001 and 111) of each bulk structure. This results in 2554 low-index surfaces. Then we searched for top, bridge and hollow active sites for N_2 binding on these surfaces by applying methods from Materials Project. The O_2 adsorbed geometries were obtained by substituting N atoms with O from the preliminary N_2 adsorbed geometries. This resulted in 905 active sites that eventually reached SCF convergence in the initial geometry optimization for both N_2 and O_2.

During the initial screening, we performed low-fidelity calculations on all candidate surfaces. For each candidate, all slab layers were fixed in initial positions to reduce computational cost, and geometry optimizations were performed with standard DFT settings to allow the N_2 and O_2 adsorbate to relax on each surface. The binding energies of both adsorbates on the surface were obtained. We expect that the adsorption energies from this approach will generally overestimate the adsorption strength, since the surface atoms are in a more reactive nonrelaxed state. Thus, only materials that exhibit more stable N_2 binding energies than O_2 were selected to enter the second round of screening.

In the second round of screening, we performed high-fidelity calculations guided by results from the initial screening. For each adsorption site identified as promising from the initial screening, the top half of the surface layers were unconstrained and additional vacuum space of 6 Å was added between each layer. Then, geometry optimization was performed via DFT to obtain the lowest N_2 and O_2 adsorption energies. Similarly to the initial screening, surfaces that exhibit more selective adsorption toward N_2 than O_2 remain in the candidate materials pool. Then, each candidate surface was visualized and examined carefully. Any surfaces with major reconstruction, adsorbate dissociation, or desorption were re-optimized with additional constraints (e.g. to prevent bond dissociation) or removed from the screening pool if no stable configurations exhibiting stronger N_2 than O_2 binding could be identified.

In the third round of screening, only three surfaces remained, two of which were based on TiO_2 bulk structures. Given the compositional similarity, we selected a single TiO_2 structure (with the strongest N_2 selectivity) and the VBO_4 structure for a final detailed study. We evaluated the feasibility of NRR on the surface by calculating the energetics of each intermediate adsorbed state involved in the NRR reaction at both GGA and hybrid levels of theory. Every NRR intermediate adsorbate from the associative NRR mechanism [7] was placed on the surface constructed from the bulk geometry and corresponding Miller indices. Geometry optimization was performed on each intermediate state using the BEEF-vdW functional, also yielding the corresponding binding energies. Vibrational frequencies and free energies are also computed using the BEEF-vdW functional. Single-point hybrid functional calculations using the HSE06 functional were performed on lowest energy intermediate state as described in Section 2.1.

All structures from each level of screening, along with scripts used for analysis and DFT simulations, are provided in the Supplementary Information (SI). The SI containing additional data, code, and materials associated with this study can be found in the GitHub repository `https://github.com/nianhant/metal_oxides_screening_for_photocatalytic_nitrogen_fixation`. The repository includes all screening data, and instruction for querying bulk structures and generating surfaces for the screening.

3 Results and Discussion

3.1 Material Screening Results

A comparison of N_2 and O_2 obtained for initial screening by low-fidelity calculations is shown in the parity plot in Fig. 1. In this initial screening, there are 6606 surface relaxations in total (total compute time of ∼500K CPU-hr), including bare and adsorbed surfaces and systems that were ultimately deemed unphysical. In this parity plot, the shaded area indicates the desired range of relative binding. Candidates within this region exhibit more favorable binding towards N_2 ($E_{N_2} \leq E_{O_2}$). These are candidate surfaces that would enter the second round of screening. These candidate metal compounds include metal species V, Mo, Sn, Zr, Sc, and Ti, and a full list is provided in the SI. The bar plot in Fig. 2 shows a comparison of the abundance of various elements before and after the first round of screening. The results indicate that there is a significant imbalance in the metal types present before and after the screening, and no strong correlation between the proportion of a given metal before and after the screening. This indicates that the screening process is identifying chemical interactions that are distinct to different metal types, rather than simply down-selecting regardless of the metals present. The bar graph also reveals that there are far more (oxy)phosphides than (oxy)borides, and despite a large number of (oxy)borides and (oxy)phosphides in the initial screening, relatively few exhibited strong N_2 adsorption.

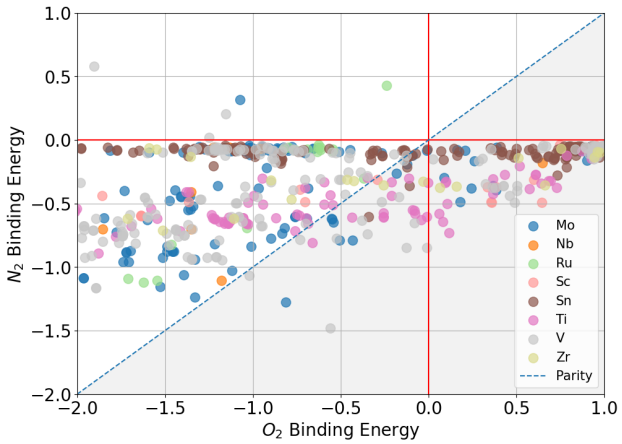

Figure 1: Parity plot of candidate surfaces' N_2 vs O_2 DFT binding energies. Scatter points **below** the parity line indicate more favorable N_2 binding. The shaded area indicates the desired range of relative binding energies, where $E_{N_2} \leq E_{O_2}$.

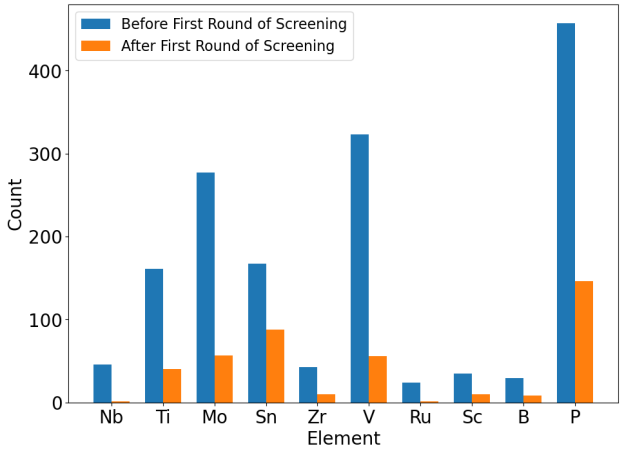

Figure 2: Number of metal oxide candidate species per element. Blue bars indicate the number of total candidates before the first round of screening, and orange bars indicate the number of qualified candidates after the first round of screening.

In the second round of screening, we performed high-fidelity geometry optimizations by allowing the top half of the slab to relax from initial positions. A total of 265 candidate adsorption sites passed the first screening round with stronger reactivity towards N_2 than O_2. A total of 804 DFT geometry optimizations were performed (∼80K CPU-hr) on these candidate sites. The relative binding energies after the second screening round are shown in Fig. 3. In many cases, significant surface reconstruction was observed during relaxation. In other cases, the surface N_2 desorbed from the active site, resulting in unstable adsorption energies. These findings are consistent with chemical intuition, since the constraints on the slab led to highly reactive surface atoms that are more prone to react with N_2, but after relaxation these surface atoms reorganize to bind with each other in the (sub)surface, making them less reactive. The criteria for the second round of screening are $E_{N_2} \leq E_{O_2}$, $E_{N_2} \leq$ -0.35 eV and $E_{O_2} \leq 0$ eV. The first criterion requires N_2 to be adsorbed onto the active site via chemisorption, with a binding energy (EN_2) of equal to or less than -0.35 eV. This threshold indicates a strong interaction between N_2 and the catalyst surface. We also implemented a criterion that ensures that the energy of O_2 adsorption (EO_2) is less than or equal to 0 eV, since positive O_2 adsorption energies are due to computational artifacts (e.g. a less stable spin state in the adsorbed O_2 calculation). None of the surfaces that were omitted due to this criterion exhibited strong N_2 adsorption, so a more detailed analysis of these structures was not carried out.

Fig. 4 shows a comparison of N_2 and O_2 binding energies between the first and second rounds of screening. The parity line represents equal binding energies for the first and second rounds of screening. Approximately 44% O_2 binding energies lie below the parity line, indicating that a considerable portion of candidate active sites exhibit stronger O_2 adsorption when the top layers of atoms are allowed to relax. On the other hand, a weaker adsorption strength towards N_2 was observed in 84% of the candidate active sites after the top layers were relaxed. This is likely due to the fact that many of the screened materials are oxides, so it is more likely that the surface reconstructions accommodate the chemisorption of O_2. The findings indicate that the screening strategy is unlikely to yield false negatives, since N_2 adsorption almost always becomes weaker, but that the lack of surface reconstruction in the first round leads to a large number of false positives.

After the second round of screening, the majority of candidates were deemed unsuitable as they did not exhibit strong and selective N_2 adsorption over O_2 adsorption. However, we identified three active sites that demonstrated the desired range of relative binding energies, as illustrated in Fig. 3. One oxyboride, VO_4B, passed the screening, but all other (oxy)borides and (oxy)phosphides were eliminated from consideration. The VO_4B surface displays the strongest N_2 adsorption (-0.85 eV), but the O_2 adsorption is nearly equal (-0.80 eV). A total of 29 (oxy)borides and 457 (oxy)phosphides were evaluated in the initial screening, with all (oxy)phosphides eliminated and one (oxy)boride identified. In comparison, 425 oxides were included in the initial screening round and two promising active sites were identified. Given the small numbers involved, it is difficult to draw strong conclusions about trends between these classes of materials, but the results suggest that (oxy)borides may be a promising class of materials for further study. Interestingly, all oxide surfaces that passed the second screening round have a bulk stoichiometry of TiO_2, although with differing bulk polymorphs and surface facets. Furthermore, the TiO_2 R3m (111) active site did not pass the second round screening criteria, but also showed strong and comparable N_2 (-0.47 eV) and O_2 (-0.50 eV) adsorption strengths. The fact that the three oxide surfaces with the strongest adsorption and selectivity towards N_2 all have TiO_2 stoichiometry suggests that there may be underlying electronic structure factors that favor interaction between N_2 and TiO_2, but a more detailed analysis is beyond the scope of this work.

The VBO_4 material identified has a modest band gap of 2.07 eV and is metastable with a formation energy 0.089 eV/atom above the hull[87], suggesting that this material is an interesting candidate for photocatalytic nitrogen conversion and suitable for a more detailed analysis. Instead of studying all TiO_2 sites in more depth, we selected the trigonal titanium oxide (001) active site that exhibits the strongest and most favorable adsorption of N_2 (-0.7 eV) over O_2 (-0.45 eV). The surface is based on the $P3_121$ space group of TiO_2, a material with a formation energy of 0.049 eV/atom above the most stable polymorph of TiO_2 and with a band gap of 3.421 eV. Given the metastable nature of the material, and the band gap that is similar to rutile and anatase titania, we conclude that it is also suitable for a more detailed study. The fact that only a few active sites pass the second round of screening reflects the difficult nature of identifying oxides that adsorb N_2 more selectively than O_2, suggesting that this is a "needle in a haystack" problem since only 3 out of 905 total active sites screened passed the second round of screening.

Given the comparison of binding energies between the first and second screening rounds, the substantial computational power needed for each round, and the rarity of successfully identifying candidate materials, this material screening scheme using fixed geometry calculations is likely impractical for the discovery of additional materials and active sites. Although computing time can be saved when all atoms are fixed, this approach neglects the overly reactive nature of some candidate surfaces, suggesting that geometry optimization is an important part of the screening pipeline. On the other hand, full geometry optimizations of all surfaces using DFT is even more computationally impractical. This suggests that novel screening approaches based on machine-learning or fast physics-based models will likely be required to identify additional active sites with strong and selective N_2 adsorption. However, as shown in the subsequent section,

the surfaces that were identified indeed exhibit strong adsorption of other intermediates and reasonable thermodynamic barriers for nitrogen reduction, suggesting that N_2 vs. O_2 selectivity is an effective descriptor for identifying surfaces that are promising for nitrogen reduction. Expanding the materials search space to include more hypothetical (oxy)borides, mixed metal oxides, or additional classes of materials that are known to selectively adsorb N_2, such as metal-organic frameworks[88–90], may also be a promising strategy for future investigations.

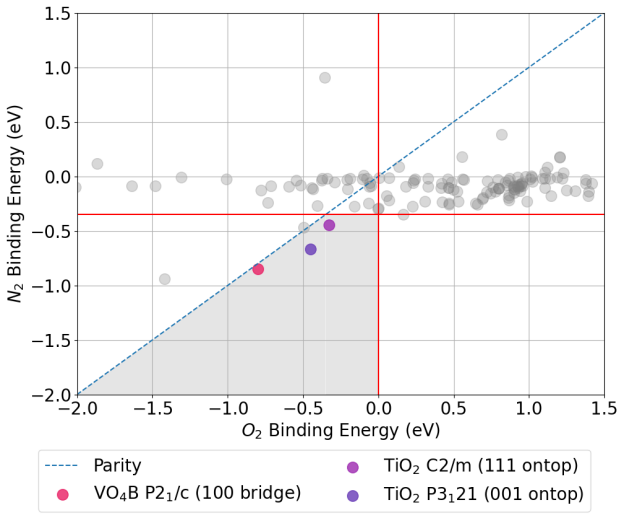

Figure 3: Parity plot of candidate surfaces' N_2 vs O_2 binding energies from the second round screening. Materials that are deemed promising after the second round screening are colored, others are grey. The shaded area indicates the desired range of relative binding energies, where $E_{N_2} \leq E_{O_2}$, $E_{N_2} \leq$ -0.35 eV and $E_{O_2} \leq 0$ eV.

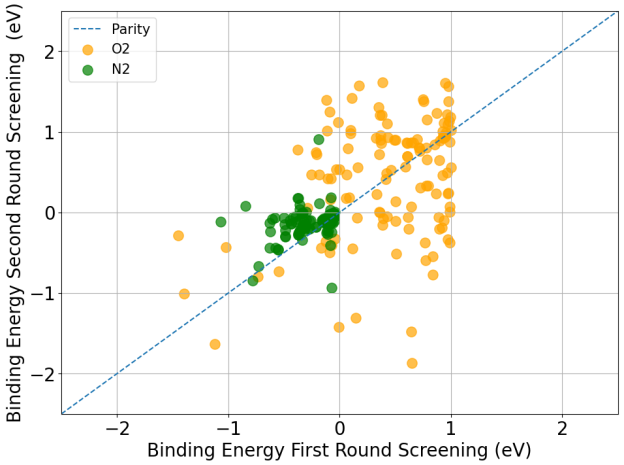

Figure 4: Parity plot of candidate surfaces' N_2 vs O_2 binding energies, before and after the second round screening.

3.2 Nitrogen Reduction Pathway on VBO_4 (100) and Trigonal TiO_2 (001)

In the third round of screening we begin by confirming the selective adsorption of N_2 at the HSE06 level of theory for both VBO_4 (100) and trigonal TiO_2 (001), since HSE06 is known to be more accurate for the treatment of gas-phase O_2. The findings are confirmed for both surfaces, with VBO_4 (100) having an N_2 adsorption free energy of -0.82 eV and O_2 adsorption energy of -0.40 eV, and trigonal TiO_2 (001) having N_2 and O_2 adsorption energies of -0.62 eV and -0.36 eV respectively. Next, we compute adsorption energies for all intermediate states in the associative NRR pathway, i.e. N_xH_y* at both the GGA (BEEF-vdW) and hybrid (HSE06) levels of theory as discussed in the methods section. The free energy diagrams can be seen in Fig. 5a, along with the free energy pathway of the associative mechanism on the proposed oxygen vacancy active site of (110) rutile TiO_2 for reference[7]. The trends in adsorption energies between the two functionals are largely consistent, although HSE06 predicts generally stronger adsorption for all species and

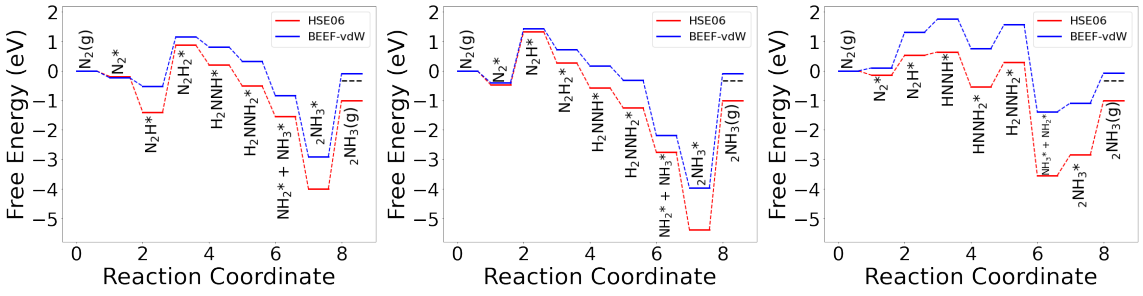

Figure 5: Free energy diagrams for the associative NRR pathway on the trigonal TiO_2 (001) active site (a), the VBO_4 (100) active site (b), and the O-br vacancy site of rutile TiO_2 (110) (c), both calculated using the BEEF-vdW and HSE06 functionals.

surfaces, and a much stronger adsorption of N_2H for trigonal TiO_2. Furthermore, HSE06 significantly overestimates the total reaction energy for NH_3 formation, while BEEF-vdW under-estimates it by a smaller margin. This indicates that although HSE06 includes Fock exchange and is expected to improve the treatment of the electronic structure of VBO_4 and TiO_2, the computed adsorption energies are not necessarily more accurate than BEEF-vdW since bonding between nitrogen and hydrogen in the gas phase has significant errors. A detailed comparison of the level of theory is beyond the scope of this work, but the fact that both follow a similar trend provides strong evidence that the qualitative conclusions are reliable.

The free energy diagram for VBO_4 is generally similar to that of the oxygen vacancy on rutile (110), with a significant thermodynamic barrier for N_2H formation, followed by exergonic steps to form strongly bound NH_3. The N_2H_2 intermediate is more stable on VBO_4 than on rutile, and the height of the thermodynamic barrier of $\sim$1.4 eV between gas-phase N_2 and N_2H is slightly lower or higher than the barrier on rutile (110), depending on the level of theory. The thermodynamic barrier for N_2H formation is significantly higher than the $\sim$0.75 eV threshold for processes that are active at room temperature [19], but the selective adsorption of N_2 and strong interaction with other intermediates suggest that other mechanisms that stabilize or avoid N_2 H may allow ammonia production on this surface. A full exploration of possible mechanisms is beyond the scope of this work, so we tentatively conclude that although the VBO_4 surface exhibits strong N_2 activity, it is not expected to be active for ammonia synthesis.

The free energy diagram for trigonal TiO_2 (001) exhibits a significant thermodynamic barriers for the conversion of N_2H to N_2H_2 (1.7 or 2.3 eV with BEEF-vdW or HSE06), as well as strongly-adsorbed NH_3. The high thermodynamic barrier for N_2H hydrogenation on the trigonal TiO_2 (001) active site is due to very stable adsorption of the $*N_2H$ intermediate state, which is in contrast to the VBO_4 and rutile (110) surfaces, where formation of N_2H is one of the most endergonic steps. Indeed, N_2H formation has been identified as the likely rate-limiting step for numerous NRR catalysts in the literature [18,91,92], indicating that the trigonal TiO_2 (001) exhibits notable stabilization of N_2H. The fact that N_2H formation is exergonic compared to the initial state suggests that under reaction conditions the N_2H coverage will likely increase, effectively increasing the free energy of the state due to configurational entropy and thus lowering the barrier for N_2H formation and providing a possible route for experimental validation via spectroscopic studies. In the limit that adsorbed N_2H is in equilibrium with the initial state (causing the free energies to be identical by definition) the barrier to N_2H_2 formation would decrease to $\sim$1 eV, bringing it close to the $\sim$0.75 eV limit needed for an active NRR catalyst [19].

The barrier that arises due to strong NH_3 adsorption exists to varying degrees for most surfaces, although NH_3 adsorption is stronger on the trigonal TiO_2 (001) surface than the VBO_4 or rutile (110) surfaces. This barrier is less important for NRR, since the free energy of gas or solution phase NH_3 will decrease at low concentrations. In the absence of significant desorption barriers, ammonia produced will equilibrate with the final state, effectively lowering this thermochemical barrier but limiting the conversion that is possible. In general, analysis of the free energy pathway suggests that the active site of trigonal TiO_2 has comparable or lower thermochemical barriers to the oxygen vacancy of rutile (110) for the conversion of N_2 to adsorbed NH_3, although more detailed investigations are needed to establish the most appropriate exchange correlation functional, explore alternative pathways such as carbon-assisted N_2 fixation [20], and identify kinetic barriers. Furthermore, it is possible that the trigonal TiO_2 (001) site exists in polycrystalline TiO_2 and works synergistically with other sites by stabilizing N_2H.

Given that nearly all the surfaces that were identified from the second round of screening (Fig. 3) are TiO_2, it is relevant to consider the stability of these surfaces to determine how likely they are to occur in polycrystalline TiO_2 or how

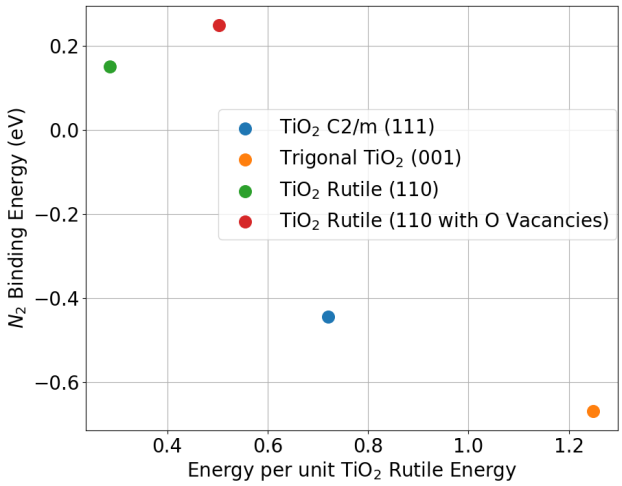

Figure 6: Surface formation energy of various candidate promising active sites vs the adsorption energy of N_2 evaluated, relative to pristine rutile (110) and rutile (110) with O vacancies.

difficult they would be to synthesize. Fig. 6 compares the N_2 adsorption and formation energies of all TiO_2 surfaces qualified in the second round of screening. The surface formation energies are computed relative to pristine rutile TiO_2, one of the most stable forms of titania. While trigonal TiO_2 displays the strongest N_2 adsorption, and the most selective N_2 adsorption over O_2, it also displays the highest surface energy. This suggests it may be difficult to synthesize and is unlikely to form spontaneously, but the fact that O_2 does not strongly adsorb or spontaneously dissociate suggests that the site will likely be meta-stable if it does form.

The trigonal TiO_2 polymorph has not been experimentally reported to our knowledge and has not been specifically tested for photocatalytic nitrogen fixation. However, other titania polymorphs and nanoparticles have been reported to photocatalytically produce ammonia in a number of studies[5,7,37,93–97], including under aerobic conditions[98]. The performance has also been reported to vary significantly depending on the polymorph and even supplier of the catalyst[37], and there are numerous inconsistent results in the literature. The presence or influence of trigonal TiO_2 active sites has never been suggested, but the meta-stable nature of the polymorph suggests that it may appear in polycrystalline titania, or that some defect sites may have a similar structure. The presence and role of these non-standard TiO_2 polymorphs and surface structures may be relevant for photocatalytic ammonia synthesis, especially under aerobic conditions. In addition, the finding suggests that intentional synthesis of the trigonal polymorph may be a promising strategy to increasing photocatalytic ammonia performance, especially if the abundance of the 001 facet[99–103] can be enhanced through capping agents or other techniques.

4 Conclusion and Future Outlook

The high-throughput DFT screening used in this work successfully identified a novel titanium dioxide active site that exhibits selective adsorption of N_2 over O_2 as well as promising energetics for the NRR reaction, and a VBO_4 active site that selectively adsorbs N_2 over O_2, but exhibits a high thermodynamic barrier for N_2H formation. The screening process revealed that surface relaxation and reconstruction can substantially affect reactivity and selectivity toward N_2, suggesting that future screening strategies should take reconstruction into account. However, the computational cost of the DFT-only screening process will likely be prohibitive for relaxations, suggesting that machine-learned force fields or other techniques should be explored. However, the findings also reveal that evaluating N_2 vs. O_2 selectivity is a promising route to substantially reduce the search space and identify active sites that are metastable and exhibit strong reactivity toward N_2.

The results of the screening process revealed several interesting active sites with TiO_2 and VBO_4 stoichiometry. Among them, the VBO_4 surface demonstrated the strongest N_2 adsorption and the trigonal TiO_2 (001) surface exhibited the strongest selectivity towards N_2. A detailed investigation of both surfaces at the GGA (BEEF-vdW) and hybrid (HSE06) levels of theory was conducted. The results show that the selective adsorption of N_2 over O_2 holds at both levels of theory, and that N_2H formation is limiting on the VBO_4 surface, while the trigonal TiO_2 surface exhibits a particularly strong reactivity toward N_2H. Free energy diagrams indicate that the trigonal TiO_2 surface exhibits a somewhat large thermochemical barriers for conversion of N_2H to N_2H_2 (1.7 or 2.3 eV for BEEF-vdW or HSE06), but these barriers

occur due to the strongly exergonic adsorption of N_2H, and may become surmountable at high N_2H coverages. These findings suggest that trigonal TiO_2 may exhibit increased photocatalytic NRR performance, or that defect sites with topologies similar to the active sites of trigonal TiO_2 (001) may contribute to photocatalytic ammonia synthesis in polycrystalline titania catalysts, especially under aerobic conditions. The findings also suggest that (oxy)borides may be a promising material class for future screening studies and that the surfaces of VBO_4 and trigonal TiO_2 surfaces may also be of interest for other applications, such as air separation. Furthermore, the fundamental chemistry underlying the selective adsorption of inert N_2 over reactive O_2 on oxide surfaces is not well understood and requires further investigation. In general, the screening process was successful in identifying an interesting trigonal TiO_2 active site structure, and revealed that surfaces capable of selectively adsorbing N_2 over O_2 are relatively rare, at least among the compounds included in this screening process.

5 Acknowledgements

The authors are grateful for funding from the National Science Foundation, under award numbers 1943707 and 1933646. We thank Prof. Phanish Suryanarayana and Xin Jing for assistance with the SPARC DFT code. We are also grateful for Georgia Institute of Technology Partnership for an Advanced Computing Environment (PACE) for the high performance computing environment.

References

[1] R. Schlögl. Catalytic synthesis of ammonia - a "never-ending story"? *Angewandte Chemie - International Edition*, 42(18):2004–2008, 2003. URL www.scopus.com. Cited By :711.

[2] Vaclav Smil. Detonator of the population explosion. *Nature*, 400(6743):415–415, jul 1999. doi: 10.1038/22672. URL http://dx.doi.org/10.1038/22672.

[3] Jens Nørskov, Jingguang Chen, Raul Miranda, Tim Fitzsimmons, and Robert Stack. Sustainable ammonia synthesis–exploring the scientific challenges associated with discovering alternative, sustainable processes for ammonia production. Technical report, US DOE Office of Science, 2016.

[4] Zachary J. Schiffer and Karthish Manthiram. Electrification and decarbonization of the chemical industry. *Joule*, 1(1):10–14, 2017. ISSN 2542-4351. doi: https://doi.org/10.1016/j.joule.2017.07.008. URL https://www.sciencedirect.com/science/article/pii/S2542435117300156.

[5] Benjamin M. Comer, Porfirio Fuentes, Christian O. Dimkpa, Yu Hsuan Liu, Carlos A. Fernandez, Pratham Arora, Matthew Realff, Upendra Singh, Marta C. Hatzell, and Andrew J. Medford. Prospects and Challenges for Solar Fertilizers, 7 2019. ISSN 25424351.

[6] Yu Hsuan Liu, Carlos A. Fernández, Sai A. Varanasi, Nhat Nguyen Bui, Likai Song, and Marta C. Hatzell. Prospects for Aerobic Photocatalytic Nitrogen Fixation. *ACS Energy Letters*, 7(1):24–29, 1 2022. ISSN 23808195. doi: 10.1021/ACSENERGYLETT.1C02260/ASSET/IMAGES/LARGE/NZ1C02260{_}0004.JPEG. URL https://pubs.acs.org/doi/full/10.1021/acsenergylett.1c02260.

[7] Benjamin M. Comer and Andrew J. Medford. Analysis of photocatalytic nitrogen fixation on rutile TiO2(110). *ACS Sustainable Chemistry & Engineering*, feb 2018. doi: 10.1021/acssuschemeng.7b03652. URL https://doi.org/10.1021%2Facssuschemeng.7b03652.

[8] Bryan H.R. Suryanto, Karolina Matuszek, Jaecheol Choi, Rebecca Y. Hodgetts, Hoang Long Du, Jacinta M. Bakker, Colin S.M. Kang, Pavel V. Cherepanov, Alexandr N. Simonov, and Douglas R. MacFarlane. Nitrogen reduction to ammonia at high efficiency and rates based on a phosphonium proton shuttle. *Science*, 372 (6547):1187–1191, 6 2021. ISSN 10959203. doi: 10.1126/SCIENCE.ABG2371/SUPPL{_}FILE/ABG2371{_}SURYANTO{_}SM.PDF. URL https://www.science.org/doi/10.1126/science.abg2371.

[9] Xiaoli Liao Etienne, Andrés Trujillo-Barrera, and Seth Wiggins. Price and volatility transmissions between natural gas, fertilizer, and corn markets. *Agricultural Finance Review*, 76(1):151–171, 5 2016. ISSN 20416326. doi: 10.1108/AFR-10-2015-0044. URL https://ideas.repec.org/a/eme/afrpps/v76y2016i1p151-171.html.

[10] Wen-Yuan. Huang, United States, Department of Agriculture., and Economic Research Service. Impact of rising natural gas prices on U.S. ammonia supply, 2007. URL https://naldc.nal.usda.gov/catalog/41854.

[11] Hazzim F. Abbas and W.M.A. Wan Daud. Hydrogen production by methane decomposition: A review. *Int. J. Hydrogen Energ.*, 35(3):1160–1190, feb 2010. doi: 10.1016/j.ijhydene.2009.11.036. URL https://doi.org/10.1016%2Fj.ijhydene.2009.11.036.

[12] M Taniguchi, M Asaaoka, and T Ayuhara. Energy saving air-separation plant based on exergy analysis. *Kobelco Technol. Rev.*, 33:34 – 38, 2015. URL https://www.scopus.com/inward/record.uri?eid=2-s2.0-85068638102&partnerID=40&md5=93bc189dff91dbef93e0b1354934267c.

[13] Benjamin M. Comer, Porfirio Fuentes, Christian O. Dimkpa, Yu-Hsuan Liu, Carlos A. Fernandez, Pratham Arora, Matthew Realff, Upendra Singh, Marta C. Hatzell, and Andrew J. Medford. Prospects and challenges for solar fertilizers. *Joule*, 3(7):1578–1605, 2019. ISSN 2542-4351. doi: https://doi.org/10.1016/j.joule.2019.05.001. URL https://www.sciencedirect.com/science/article/pii/S2542435119302132.

[14] Andrew J. Medford and Marta C. Hatzell. Photon-driven nitrogen fixation: Current progress, thermodynamic considerations, and future outlook. *ACS Catalysis*, 7(4):2624–2643, 2017. doi: 10.1021/acscatal.7b00439. URL https://doi.org/10.1021/acscatal.7b00439.

[15] Natasha Gilbert. African agriculture: Dirt poor. *Nature*, 483(7391):525–527, mar 2012. doi: 10.1038/483525a. URL http://dx.doi.org/10.1038/483525a.

[16] Shiming Chen, Siglinda Perathoner, Claudio Ampelli, Chalachew Mebrahtu, Dangsheng Su, and Gabriele Centi. Electrocatalytic Synthesis of Ammonia at Room Temperature and Atmospheric Pressure from Water and Nitrogen on a Carbon-Nanotube-Based Electrocatalyst. *Angewandte Chemie*, 129(10):2743–2747, 3 2017. ISSN 1521-3757. doi: 10.1002/ANGE.201609533. URL https://onlinelibrary.wiley.com/doi/full/10.1002/ange.201609533https://onlinelibrary.wiley.com/doi/abs/10.1002/ange.201609533https://onlinelibrary.wiley.com/doi/10.1002/ange.201609533.

[17] Jingguang G. Chen, Richard M. Crooks, Lance C. Seefeldt, Kara L. Bren, R. Morris Bullock, Marcetta Y. Darensbourg, Patrick L. Holland, Brian Hoffman, Michael J. Janik, Anne K. Jones, Mercouri G. Kanatzidis, Paul King, Kyle M. Lancaster, Sergei V. Lymar, Peter Pfromm, William F. Schneider, and Richard R. Schrock. Beyond fossil fuel–driven nitrogen transformations. *Science*, 360(6391), 5 2018. ISSN 10959203. doi: 10.1126/SCIENCE.AAR6611/ASSET/E2BD967E-A5CA-4DD3-8F9B-487DDB1B1BDA/ASSETS/GRAPHIC/360{_}AAR6611{_}F4.JPEG. URL https://www.science.org/doi/10.1126/science.aar6611.

[18] Egill Skulason, Thomas Bligaard, Sigrídur Gudmundsdóttir, Felix Studt, Jan Rossmeisl, Frank Abild-Pedersen, Tejs Vegge, Hannes Jónsson, and Jens K Nørskov. A theoretical evaluation of possible transition metal electro-catalysts for n 2 reduction. *Phys. Chem. Chem. Phys.*, 14(3):1235–1245, 2012.

[19] Haldrian Iriawan, Suzanne Z. Andersen, Xilun Zhang, Benjamin M. Comer, Jesús Barrio, Ping Chen, Andrew J. Medford, Ifan E. L. Stephens, Ib Chorkendorff, and Yang Shao-Horn. Methods for nitrogen activation by reduction and oxidation. *Nature Reviews Methods Primers*, 1(1):56, Aug 2021. ISSN 2662-8449. doi: 10.1038/s43586-021-00053-y. URL https://doi.org/10.1038/s43586-021-00053-y.

[20] Benjamin M. Comer, Yu Hsuan Liu, Marm B. Dixit, Kelsey B. Hatzell, Yifan Ye, Ethan J. Crumlin, Marta C. Hatzell, and Andrew J. Medford. The Role of Adventitious Carbon in Photo-catalytic Nitrogen Fixation by Titania. *Journal of the American Chemical Society*, 140(45):15157–15160, 11 2018. ISSN 15205126. doi: 10.1021/jacs.8b08464.

[21] Benjamin M. Comer and Andrew J. Medford. Analysis of Photocatalytic Nitrogen Fixation on Rutile TiO2(110). *ACS Sustainable Chemistry and Engineering*, 6(4):4648–4660, 4 2018. ISSN 21680485. doi: 10.1021/acssuschemeng.7b03652.

[22] Joseph H. Montoya, Charlie Tsai, Aleksandra Vojvodic, and Jens K. Nørskov. The Challenge of Electrochemical Ammonia Synthesis: A New Perspective on the Role of Nitrogen Scaling Relations. *ChemSusChem*, 8(13):2180–2186, 7 2015. ISSN 1864-564X. doi: 10.1002/CSSC.201500322. URL https://onlinelibrary.wiley.com/doi/full/10.1002/cssc.201500322https://onlinelibrary.wiley.com/doi/abs/10.1002/cssc.201500322https://chemistry-europe.onlinelibrary.wiley.com/doi/full/10.1002/cssc.201500322.

[23] Andrew J. Medford and Marta C. Hatzell. Photon-Driven Nitrogen Fixation: Current Progress, Thermodynamic Considerations, and Future Outlook, 4 2017. ISSN 21555435.

[24] Aleksandra Vojvodic, Andrew James Medford, Felix Studt, Frank Abild-Pedersen, Tuhin Suvra Khan, T. Bligaard, and J. K. Nørskov. Exploring the limits: A low-pressure, low-temperature Haber–Bosch process. *Chemical Physics Letters*, 598:108–112, 4 2014. ISSN 0009-2614. doi: 10.1016/J.CPLETT.2014.03.003.

[25] Xiao-Ying Xie, Pin Xiao, Wei-Hai Fang, Ganglong Cui, and Walter Thiel. Probing photocatalytic nitrogen reduction to ammonia with water on the rutile tio2 (110) surface by first-principles calculations. *ACS Catalysis*, 9(10):9178–9187, 2019. doi: 10.1021/acscatal.9b01551. URL https://doi.org/10.1021/acscatal.9b01551.

[26] Jimmie G Edwards, Julian A Davies, David L Boucher, and Abdelkader Mennad. An Opinion on the Heterogeneous Photoreactions of N2 with H2O. *Angew. Chem. Int. Ed.*, 31(4):480–482, 1992.

[27] R. Schaub, P. Thostrup, N. Lopez, E. Lægsgaard, I. Stensgaard, J. K. Nørskov, and F. Besenbacher. Oxygen vacancies as active sites for water dissociation on rutile TiO 2 (110). *Phys. Rev. Lett.*, 87(26), dec 2001. doi: 10.1103/physrevlett.87.266104. URL http://dx.doi.org/10.1103/physrevlett.87.266104.

[28] Michael A. Henderson. An HREELS and TPD study of water on TiO2(110): the extent of molecular versus dissociative adsorption. *Surface Science*, 355(1-3):151–166, 1996. ISSN 00396028. doi: 10.1016/0039-6028(95)01357-1. URL http://linkinghub.elsevier.com/retrieve/pii/0039602895013571.

[29] S Krischok, O Höfft, J Günster, J Stultz, D.W Goodman, and V Kempter. H2o interaction with bare and li-precovered TiO2: studies with electron spectroscopies (MIES and UPS(HeI and II)). *Surface Science*, 495(1-2):8–18, dec 2001. doi: 10.1016/s0039-6028(01)01570-9. URL https://doi.org/10.1016%2Fs0039-6028%2801%2901570-9.

[30] Guido Ketteler, Susumu Yamamoto, Hendrik Bluhm, Klas Andersson, David E. Starr, D. Frank Ogletree, Hirohito Ogasawara, Anders Nilsson, and Miquel Salmeron. The nature of water nucleation sites on TiO2(110) surfaces revealed by ambient pressure x-ray photoelectron spectroscopy. *The Journal of Physical Chemistry C*, 111(23):8278–8282, jun 2007. doi: 10.1021/jp068606i. URL https://doi.org/10.1021%2Fjp068606i.

[31] Benjamin M. Comer, Yu-Hsuan Liu, Marm B. Dixit, Kelsey B. Hatzell, Yifan Ye, Ethan J. Crumlin, Marta C. Hatzell, and Andrew J. Medford. The role of adventitious carbon in photo-catalytic nitrogen fixation by titania. *Journal of the American Chemical Society*, 140(45):15157–15160, 2018. doi: 10.1021/jacs.8b08464. URL https://doi.org/10.1021/jacs.8b08464. PMID: 30372055.

[32] Po-Wei Huang, Nianhan Tian, Tijana Rajh, Yu-Hsuan Liu, Giada Innocenti, Carsten Sievers, Andrew J Medford, and Marta C Hatzell. Formation of carbon-induced nitrogen-centered radicals on titanium dioxide under illumination. 6 2023. doi: 10.26434/CHEMRXIV-2023-00C51. URL https://chemrxiv.org/engage/chemrxiv/article-details/648e1e74be16ad5c5713e605.

[33] Jeffrey Ralph Bartels. A feasibility study of implementing an Ammonia Economy. Technical report, 2008.

[34] Collin Smith, Alfred K Hill, and Laura Torrente-Murciano. Current and future role of haber–bosch ammonia in a carbon-free energy landscape. *Energy & Environmental Science*, 13(2):331–344, 2020.

[35] Max Appl. Ammonia, 2. Production Processes. *Ullmann's Encyclopedia of Industrial Chemistry*, 10 2011. ISSN 1435-6007. doi: 10.1002/14356007.O02{_}O11. URL https://onlinelibrary.wiley.com/doi/full/10.1002/14356007.o02_o11https://onlinelibrary.wiley.com/doi/abs/10.1002/14356007.o02_o11https://onlinelibrary.wiley.com/doi/10.1002/14356007.o02_o11.

[36] Brian A. Rohr, Aayush R. Singh, and Jens K. Nørskov. A theoretical explanation of the effect of oxygen poisoning on industrial Haber-Bosch catalysts. *Journal of Catalysis*, 372:33–38, 4 2019. ISSN 0021-9517. doi: 10.1016/J.JCAT.2019.01.042.

[37] Hiroaki Hirakawa, Masaki Hashimoto, Yasuhiro Shiraishi, and Takayuki Hirai. Photocatalytic conversion of nitrogen to ammonia with water on surface oxygen vacancies of titanium dioxide. *Journal of the American Chemical Society*, 139(31):10929–10936, jul 2017. doi: 10.1021/jacs.7b06634. URL https://doi.org/10.1021%2Fjacs.7b06634.

[38] Liqun Ye, Chunqiu Han, Zhaoyu Ma, Yumin Leng, Jue Li, Xiaoxu Ji, Dongqin Bi, Haiquan Xie, and Zixuan Huang. Ni2P loading on Cd0.5Zn0.5S solid solution for exceptional photocatalytic nitrogen fixation under visible light. *Chemical Engineering Journal*, 307:311–318, 1 2017. ISSN 1385-8947. doi: 10.1016/J.CEJ.2016.08.102.

[39] Hao Huang, Xu Sheng Wang, Davin Philo, Fumihiko Ichihara, Hui Song, Yunxiang Li, Dan Li, Teng Qiu, Shengyao Wang, and Jinhua Ye. Toward visible-light-assisted photocatalytic nitrogen fixation: A titanium metal organic framework with functionalized ligands. *Applied Catalysis B: Environmental*, 267:118686, 6 2020. ISSN 0926-3373. doi: 10.1016/J.APCATB.2020.118686.

[40] Katja Li, Suzanne Z. Andersen, Michael J. Statt, Mattia Saccoccio, Vanessa J. Bukas, Kevin Krempl, Rokas Sažinas, Jakob B. Pedersen, Vahid Shadravan, Yuanyuan Zhou, Debasish Chakraborty, Jakob Kibsgaard, Peter C.K. Vesborg, Jens K. Nørskov, and Ib Chorkendorff. Enhancement of lithium-mediated ammonia synthesis by addition of oxygen. *Science*, 374(6575):1593–1597, 12 2021. ISSN 10959203. doi: 10.1126/SCIENCE.ABL4300/SUPPL{_}FILE/SCIENCE.ABL4300{_}SM.PDF. URL https://www.science.org/doi/10.1126/science.abl4300.

[41] Ali Hussain Motagamwala and James A. Dumesic. Microkinetic Modeling: A Tool for Rational Catalyst Design. *Chemical Reviews*, 121(2):1049–1076, 1 2021. ISSN 15206890. doi: 10.1021/ACS.CHEMREV.0C00394/ASSET/IMAGES/MEDIUM/CR0C00394{_}M051.GIF. URL https://pubs.acs.org/doi/full/10.1021/acs.chemrev.0c00394.

[42] Andrew A. Peterson, Frank Abild-Pedersen, Felix Studt, Jan Rossmeisl, and Jens K. Nørskov. How copper catalyzes the electroreduction of carbon dioxide into hydrocarbon fuels. *Energy & Environmental Science*, 3(9): 1311, 2010. doi: 10.1039/c0ee00071j. URL https://doi.org/10.1039%2Fc0ee00071j.

[43] Brook Wander, Kirby Broderick, and Zachary W. Ulissi. Catlas: an automated framework for catalyst discovery demonstrated for direct syngas conversion. *Catalysis Science & Technology*, 2022. ISSN 2044-4753. doi: 10.1039/d2cy01267g.

[44] Anubhav Jain, Shyue Ping Ong, Geoffroy Hautier, Wei Chen, William Davidson Richards, Stephen Dacek, Shreyas Cholia, Dan Gunter, David Skinner, Gerbrand Ceder, and Kristin a. Persson. The Materials Project: A materials genome approach to accelerating materials innovation. *APL Materials*, 1(1):011002, 2013. ISSN 2166532X. doi: 10.1063/1.4812323. URL http://link.aip.org/link/AMPADS/v1/i1/p011002/s1&Agg=doi.

[45] The Materials Project. Materials data on tio2 by materials project. doi: 10.17188/1267616.

[46] Chengliang Mao, Jiaxian Wang, Yunjie Zou, Hao Li, Guangming Zhan, Jie Li, Jincai Zhao, and Lizhi Zhang. Anion (o, n, c, and s) vacancies promoted photocatalytic nitrogen fixation. *Green Chemistry*, 21(11):2852–2867, 2019.

[47] Chengcheng Li, Tuo Wang, Zhi-Jian Zhao, Weimin Yang, Jian-Feng Li, Ang Li, Zhilin Yang, Geoffrey A. Ozin, and Jinlong Gong. Promoted fixation of molecular nitrogen with surface oxygen vacancies on plasmon-enhanced TiO2 photoelectrodes. *Angewandte Chemie International Edition*, mar 2018. doi: 10.1002/anie.201713229. URL https://doi.org/10.1002%2Fanie.201713229.

[48] Ting Zheng, Chunya Wu, Mingjun Chen, Yu Zhang, and Peter T. Cummings. A DFT study of water adsorption on rutile TiO2 (110) surface: The effects of surface steps. *The Journal of Chemical Physics*, 145(4):044702, jul 2016. doi: 10.1063/1.4958969. URL http://dx.doi.org/10.1063/1.4958969.

[49] Peter Deák, Bálint Aradi, and Thomas Frauenheim. Polaronic effects in TiO 2 calculated by the HSE06 hybrid functional: Dopant passivation by carrier self-trapping. *Phys. Rev. B*, 83(15), apr 2011. doi: 10.1103/physrevb.83.155207. URL http://dx.doi.org/10.1103/physrevb.83.155207.

[50] Sushree Jagriti Sahoo, Xin Jing, Phanish Suryanarayana, and Andrew J. Medford. Ab-Initio Investigation of Finite Size Effects in Rutile Titania Nanoparticles with Semilocal and Nonlocal Density Functionals. *Journal of Physical Chemistry C*, 126(4):2121–2130, 2 2022. ISSN 19327455. doi: 10.1021/ACS.JPCC.1C08915/ASSET/IMAGES/LARGE/JP1C08915{_}0006.JPEG. URL https://pubs.acs.org/doi/full/10.1021/acs.jpcc.1c08915.

[51] Jess Wellendorff, Keld T. Lundgaard, Andreas Møgelhøj, Vivien Petzold, David D. Landis, Jens K. Nørskov, Thomas Bligaard, and Karsten W. Jacobsen. Density functionals for surface science: Exchange-correlation model development with bayesian error estimation. *Physical Review B*, 85(23):235149–235149, 2012. doi: 10.1103/PhysRevB.85.235149.

[52] Paolo Giannozzi, Stefano Baroni, Nicola Bonini, Matteo Calandra, Roberto Car, Carlo Cavazzoni, Davide Ceresoli, Guido L Chiarotti, Matteo Cococcioni, Ismaila Dabo, Andrea Dal Corso, Stefano de Gironcoli, Stefano Fabris, Guido Fratesi, Ralph Gebauer, Uwe Gerstmann, Christos Gougoussis, Anton Kokalj, Michele Lazzeri, Layla Martin-Samos, Nicola Marzari, Francesco Mauri, Riccardo Mazzarello, Stefano Paolini, Alfredo Pasquarello, Lorenzo Paulatto, Carlo Sbraccia, Sandro Scandolo, Gabriele Sclauzero, Ari P Seitsonen, Alexander Smogunov, Paolo Umari, and Renata M Wentzcovitch. Quantum espresso: a modular and open-source software project for quantum simulations of materials. *Journal of Physics: Condensed Matter*, 21(39):395502 (19pp), 2009. URL http://www.quantum-espresso.org.

[53] Advanced capabilities for materials modelling with Quantum ESPRESSO. 2017. doi: 10.1088/1361-648X/aa8f79. URL https://doi.org/10.1088/1361-648X/aa8f79.

[54] Ask Hjorth Larsen, Jens Jørgen Mortensen, Jakob Blomqvist, Ivano E Castelli, Rune Christensen, Marcin Dułak, Jesper Friis, Michael N Groves, Bjørk Hammer, Cory Hargus, et al. The atomic simulation environment—a python library for working with atoms. *Journal of Physics: Condensed Matter*, 29(27):273002, 2017.

[55] Hendrik J. Monkhorst and James D. Pack. Special points for brillouin-zone integrations. *Physical Review B*, 13 (12):5188–5192, jun 1976. doi: 10.1103/physrevb.13.5188. URL https://doi.org/10.1103%2Fphysrevb.13.5188.

[56] Gianluca Prandini, Antimo Marrazzo, Ivano E. Castelli, Nicolas Mounet, Elsa Passaro, and Nicola Marzari. A Standard Solid State Pseudopotentials (SSSP) library optimized for precision and efficiency, 11 2020.

[57] Lennart Bengtsson. Dipole correction for surface supercell calculations. *Physical Review B*, 59(19):12301–12304, may 1999. doi: 10.1103/physrevb.59.12301. URL https://doi.org/10.1103%2Fphysrevb.59.12301.

[58] Jochen Heyd, Gustavo E. Scuseria, and Matthias Ernzerhof. Hybrid functionals based on a screened coulomb potential. *The Journal of Chemical Physics*, 118(18):8207–8215, 2003. doi: 10.1063/1.1564060. URL https://doi.org/10.1063/1.1564060.

[59] Swarnava Ghosh and Phanish Suryanarayana. Sparc: Accurate and efficient finite-difference formulation and parallel implementation of density functional theory: Extended systems. *Computer Physics Communications*, 216:109–125, 2017. ISSN 0010-4655. doi: https://doi.org/10.1016/j.cpc.2017.02.019. URL https://www.sciencedirect.com/science/article/pii/S0010465517300711.

[60] Swarnava Ghosh and Phanish Suryanarayana. SPARC: Accurate and efficient finite-difference formulation and parallel implementation of Density Functional Theory: Isolated clusters. *Computer Physics Communications*, 212:189–204, 3 2017. ISSN 00104655. doi: 10.1016/j.cpc.2016.09.020.

[61] Qimen Xu, Abhiraj Sharma, Benjamin Comer, Hua Huang, Edmond Chow, Andrew J. Medford, John E. Pask, and Phanish Suryanarayana. SPARC: Simulation Package for Ab-initio Real-space Calculations. *SoftwareX*, 15: 100709, 7 2021. ISSN 2352-7110. doi: 10.1016/J.SOFTX.2021.100709.

[62] Mostafa Faghih Shojaei, John E. Pask, Andrew J. Medford, and Phanish Suryanarayana. Soft and transferable pseudopotentials from multi-objective optimization. 9 2022. doi: 10.48550/arxiv.2209.09806. URL http://arxiv.org/abs/2209.09806.

[63] Phanish Suryanarayana, Phanisri P. Pratapa, and John E. Pask. Alternating Anderson–Richardson method: An efficient alternative to preconditioned Krylov methods for large, sparse linear systems. *Computer Physics Communications*, 234:278–285, 1 2019. ISSN 0010-4655. doi: 10.1016/J.CPC.2018.07.007.

[64] Phanisri P Pratapa, Phanish Suryanarayana, and John E Pask. Anderson acceleration of the Jacobi iterative method: An efficient alternative to Krylov methods for large, sparse linear systems. *Journal of Computational Physics*, 306:43–54, 2016. ISSN 0021-9991. doi: https://doi.org/10.1016/j.jcp.2015.11.018. URL https://www.sciencedirect.com/science/article/pii/S0021999115007585.

[65] Amartya S Banerjee, Phanish Suryanarayana, and John E Pask. Periodic Pulay method for robust and efficient convergence acceleration of self-consistent field iterations. *Chemical Physics Letters*, 647:31–35, 2016. ISSN 0009-2614. doi: https://doi.org/10.1016/j.cplett.2016.01.033. URL https://www.sciencedirect.com/science/article/pii/S0009261416000464.

[66] Shashikant Kumar, Qimen Xu, and Phanish Suryanarayana. On preconditioning the self-consistent field iteration in real-space Density Functional Theory. *Chemical Physics Letters*, 739:136983, 2020. ISSN 0009-2614. doi: https://doi.org/10.1016/j.cplett.2019.136983. URL https://www.sciencedirect.com/science/article/pii/S0009261419309649.

[67] Phanisri P Pratapa and Phanish Suryanarayana. Restarted Pulay mixing for efficient and robust acceleration of fixed-point iterations. *Chemical Physics Letters*, 635:69–74, 2015. ISSN 0009-2614. doi: https://doi.org/10.1016/j.cplett.2015.06.029. URL https://www.sciencedirect.com/science/article/pii/S0009261415004480.

[68] URL http://cmt.dur.ac.uk/sjc/thesis/thesis/node14.html.

[69] The Abinit group. Geometric considerations¶. URL https://docs.abinit.org/theory/geometry/.

[70] Aliaksandr V. Krukau, Oleg A. Vydrov, Artur F. Izmaylov, and Gustavo E. Scuseria. Influence of the exchange screening parameter on the performance of screened hybrid functionals. *The Journal of Chemical Physics*, 125 (22):224106, 12 2006. ISSN 0021-9606. doi: 10.1063/1.2404663. URL https://aip.scitation.org/doi/abs/10.1063/1.2404663.

[71] Rasmus Y. Brogaard, Reynald Henry, Yves Schuurman, Andrew J. Medford, Poul Georg Moses, Pablo Beato, Stian Svelle, Jens K. Nørskov, and Unni Olsbye. Methanol-to-hydrocarbons conversion: The alkene methylation pathway. *Journal of Catalysis*, 314:159–169, 2014. ISSN 0021-9517. doi: https://doi.org/10.1016/j.jcat.2014.04.006. URL https://www.sciencedirect.com/science/article/pii/S0021951714000864.

[72] Karsten Reuter, Catherine Stampf, and Matthias Scheffler. AB initio atomistic thermodynamics and statistical mechanics of surface properties and functions. In *Handbook of Materials Modeling*, pages 149–194. Springer Nature, 2005. doi: 10.1007/1-4020-3286-2_10. URL https://doi.org/10.1007%2F1-4020-3286-2_10.

[73] GN Schrauzer and TD Guth. Photocatalytic reactions. 1. Photolysis of water and photoreduction of nitrogen on titanium dioxide. *J. Am. Chem. Soc.*, 99(22):7189–7193, 1977.

[74] Gerhard N Schrauzer. Photoreduction of Nitrogen on TiO2 and TiO2-Containing Minerals. In *Energy Efficiency and Renewable Energy Through Nanotechnology*, pages 601–623. Springer, 2011.

[75] GN Schrauzer, TD Guth, J Salehi, N Strampach, Liu Nan Hui, and MR Palmer. Homogeneous and heterogeneous photocatalysis. *by D. Reidel Publishing Company*, page 509, 1986.

[76] Chongyi Ling, Xiaowan Bai, Yixin Ouyang, Aijun Du, and Jinlan Wang. Single molybdenum atom anchored on n-doped carbon as a promising electrocatalyst for nitrogen reduction into ammonia at ambient conditions. *The Journal of Physical Chemistry C*, 122(29):16842–16847, 2018.

[77] D. V. Yandulov. Catalytic reduction of dinitrogen to ammonia at a single molybdenum center. *Science*, 301(5629): 76–78, jul 2003. doi: 10.1126/science.1085326. URL https://doi.org/10.1126%2Fscience.1085326.

[78] Shogo Kuriyama, Kazuya Arashiba, Kazunari Nakajima, Hiromasa Tanaka, Nobuaki Kamaru, Kazunari Yoshizawa, and Yoshiaki Nishibayashi. Catalytic formation of ammonia from molecular dinitrogen by use of dinitrogen-bridged dimolybdenum–dinitrogen complexes bearing pnp-pincer ligands: remarkable effect of substituent at pnp-pincer ligand. *Journal of the American Chemical Society*, 136(27):9719–9731, 2014.

[79] Javier Fajardo Jr and Jonas C Peters. Catalytic nitrogen-to-ammonia conversion by osmium and ruthenium complexes. *Journal of the American Chemical Society*, 139(45):16105–16108, 2017.

[80] Shelby L. Foster, Sergio I.Perez Bakovic, Royce D. Duda, Sharad Maheshwari, Ross D. Milton, Shelley D. Minteer, Michael J. Janik, Julie N. Renner, and Lauren F. Greenlee. Catalysts for nitrogen reduction to ammonia. *Nature Catalysis 2018 1:7*, 1(7):490–500, 7 2018. ISSN 2520-1158. doi: 10.1038/s41929-018-0092-7. URL https://www.nature.com/articles/s41929-018-0092-7.

[81] Xuan Yang, Jared Nash, Jacob Anibal, Marco Dunwell, Shyam Kattel, Eli Stavitski, Klaus Attenkofer, Jingguang G Chen, Yushan Yan, and Bingjun Xu. Mechanistic insights into electrochemical nitrogen reduction reaction on vanadium nitride nanoparticles. *Journal of the American Chemical Society*, 140(41):13387–13391, 2018.

[82] Pengxiang Li, Wenzhi Fu, Peiyuan Zhuang, Yudong Cao, Can Tang, Angelica Blake Watson, Pei Dong, Jianfeng Shen, and Mingxin Ye. Amorphous sn/crystalline sns2 nanosheets via in situ electrochemical reduction methodology for highly efficient ambient n2 fixation. *Small*, 15(40):1902535, 2019.

[83] Chunjin Ren, Qianyu Jiang, Wei Lin, Yongfan Zhang, Shuping Huang, and Kaining Ding. Density functional theory study of single-atom v, nb, and ta catalysts on graphene and carbon nitride for selective nitrogen reduction. *ACS Applied Nano Materials*, 3(6):5149–5159, 2020.

[84] Jiabin Tan, Xiaobo He, Fengxiang Yin, Xin Liang, Guoru Li, and Zhichun Li. Zr-doped α-feooh with high faradaic efficiency for electrochemical nitrogen reduction reaction. *Applied Surface Science*, 567:150801, 2021.

[85] Lars H. Jepsen, Morten B. Ley, Young Su Lee, Young Whan Cho, Martin Dornheim, Jens Oluf Jensen, Yaroslav Filinchuk, Jens Erik Jørgensen, Flemming Besenbacher, and Torben R. Jensen. Boron–nitrogen based hydrides and reactive composites for hydrogen storage. *Materials Today*, 17(3):129–135, 4 2014. ISSN 1369-7021. doi: 10.1016/J.MATTOD.2014.02.015.

[86] Marc André Légaré, Guillaume Bélanger-Chabot, Rian D. Dewhurst, Eileen Welz, Ivo Krummenacher, Bernd Engels, and Holger Braunschweig. Nitrogen fixation and reduction at boron. *Science (New York, N.Y.)*, 359 (6378):896–900, 2 2018. ISSN 1095-9203. doi: 10.1126/SCIENCE.AAQ1684. URL https://pubmed.ncbi.nlm.nih.gov/29472479/.

[87] Mp-553432: Tio2 (trigonal, p$3_121, 152$). URL.

Xue Han, Sihai Yang, and Martin Schröder. Metal–Organic Framework Materials for Production and Distribution of Ammonia. *Journal of the American Chemical Society*, 145(4):1998–2012, 1 2023. 10.1021/jacs.2c06216.

Islam E Khalil, Cong Xue, Wenjing Liu, Xiaohan Li, Yu Shen, Sheng Li, Weina Zhang, Fengwei Huo, I E Khalil, C Xue, W Liu, X Li, Y Shen, S Li, W Zhang, and F Huo. The Role of Defects in Metal-Organic Frameworks for Nitrogen Reduction Reaction: When Defects Switch to Features. 2021. 10.1002/adfm.202010052. URL https://onlinelibrary.wiley.com/doi/10.1002/adfm.202010052.

Bo Han, Jiawei Liu, Carmen Lee, Chade Lv, and Qingyu Yan. REVIEW www.small-methods.com Recent Advances in Metal-Organic Framework-Based Nanomaterials for Electrocatalytic Nitrogen Reduction. 2023. 10.1002/smtd.202300277. URL https://onlinelibrary.wiley.com/doi/10.1002/smtd.202300277.

Yongfei Ji, Paiyong Liu, and Ting Fan. Unifying the Nitrogen Reduction Activity of Anatase and Rutile TiO2 Surfaces. *ChemPhysChem*, 24(2):e202200653, 1 2023. ISSN 1439-7641. 10.1002/CPHC.202200653. URL https://onlinelibrary.wiley.com/doi/full/10.1002/cphc.202200653https://onlinelibrary.wiley.com/doi/abs/10.1002/cphc.202200653https://chemistry-europe.onlinelibrary.wiley.com/doi/full/10.1002/cphc.202200653.

S. Bourgeois, D. Diakite, and M. Perdereau. A study of TiO2 powders as a support for the photochemical synthesis of ammonia. *Reactivity of Solids*, 6(1):95–104, 10 1988. ISSN 0168-7336. 10.1016/0168-7336(88)80048-2.

G Lu, a Linsebigler, and J T Yates. Ti3+ Defect Sites on TiO2(110): Production and Chemical Detection of Active Sites. *Journal of Physical Chemistry*, 98(45):11733–11738, 1994. ISSN 0022-3654. 10.1021/j100096a017. URL http://pubs.acs.org/doi/abs/10.1021/j100096a017.

Safia Benkoula, Olivier Sublemontier, Minna Patanen, Christophe Nicolas, Fausto Sirotti, Ahmed Naitabdi, François Gaie-Levrel, Egill Antonsson, Damien Aureau, François-Xavier Ouf, Shin-Ichi Wada, Arnaud Etcheberry, Kiyoshi Ueda, and Catalin Miron. Water adsorption on TiO2 surfaces probed by soft X-ray spectroscopies: bulk materials vs. isolated nanoparticles. *Scientific Reports*, 5(January):15088, 2015. ISSN 2045-2322. 10.1038/srep15088. URL http://www.nature.com/articles/srep15088.

C. N. Rusu and J. T. Yates Jr. N2O Adsorption and Photochemistry on High Area TiO2 Powder. *J. Phys. Chem. B*, 105 (13):2596–2603, 2001. ISSN 1520-6106. 10.1021/jp0040345. URL http://pubs.acs.org/doi/abs/10.1021/jp0040345.

Michael A. Henderson. A surface science perspective on TiO2 photocatalysis. *Surface Science Reports*, 66(6-7):185–297, jun 2011. 10.1016/j.surfrep.2011.01.001. URL https://doi.org/10.1016%2Fj.surfrep.2011.01.001.

Daojian Cheng, Jianhui Lan, Dapeng Cao, and Wenchuan Wang. Adsorption and dissociation of ammonia on clean and metal-covered TiO2 rutile (110) surfaces: A comparative DFT study. *Applied Catalysis B: Environmental*, 106(3-4): 510–519, 2011. ISSN 09263373. 10.1016/j.apcatb.2011.06.010. URL http://dx.doi.org/10.1016/j.apcatb.2011.06.010.

Yu-Hsuan Liu, Carlos A. Fernández, Sai A. Varanasi, Nhat Nguyen Bui, Likai Song, and Marta C. Hatzell. Prospects for aerobic photocatalytic nitrogen fixation. *ACS Energy Letters*, 7(1):24–29, 2022. 10.1021/acsenergylett.1c02260. URL https://doi.org/10.1021/acsenergylett.1c02260.

Nitish Roy, Youngku Sohn, and Debabrata Pradhan. Synergy of Low-Energy {101} and High-Energy {001} TiO2 Crystal Facets for Enhanced Photocatalysis. *ACS Nano*, 7(3):2532–2540, 3 2013. 10.1021/nn305877v.

Evgeny V Kislov, Svyatoslav V Luchnikov, Nadezhda V Selezneva, and Nikolai V Baranov. Effect of titanium and titanium dioxide doping on the superconducting properties of the Fe 1.02 Se compound ARTICLES YOU MAY BE INTERESTED IN Effect of Titanium and Titanium Dioxide Doping on the Superconducting Properties of the Fe 1.02 Se Compound. 2466:30028, 2022. 10.1063/5.0088764. URL https://doi.org/10.1063/5.0088764.

Seung Yong Chae, Myun Kyu Park, Sang Kyung Lee, Taek Young Kim, Sang Kyu Kim, and Wan In Lee. Preparation of Size-Controlled TiO2 Nanoparticles and Derivation of Optically Transparent Photocatalytic Films. *Chemistry of Materials*, 15(17):3326–3331, 7 2003. 10.1021/cm030171d.

Yulong Liao, Huaiwu Zhang, Wenxiu Que, Peng Zhong, Feiming Bai, Zhiyong Zhong, Qiye Wen, and Wenhao Chen. Activating the Single-Crystal TiO2 Nanoparticle Film with Exposed {001} Facets. *ACS Applied Materials & Interfaces*, 5(14):6463–6466, 7 2013. 10.1021/am401869e.

Yu Yu, Changyan Cao, Wei Li, Ping Li, Jin Qu, and Weiguo Song. Low-cost synthesis of robust anatase polyhedral structures with a preponderance of exposed {001} facets for enhanced photoactivities. *Nano Research*, 5(6):434–442, 5 2012. ISSN 19980000. 10.1007/S12274-012-0226-1/METRICS. URL https://link.springer.com/article/10.1007/s12274-012-0226-1.